Material models for concrete exposed to impact loading

Henrik Sjøl

Material models for concrete
exposed to impact loading

Henrik Sjøl

Summary

Concrete is an important material in building protective structures. To calculate what happens to these structures when exposed to impact loads, we need to have a good understanding of the material behavior. Empirical and theoretical models to estimate penetration depth include only compressive strength and density. When performing a numerical simulation, a more detailed description is needed. In this report, an overview over different material models for concrete is given.

Concrete is an inhomogeneous material. It consists of mortar, aggregate and in many cases reinforcement. In the literature, there exist several models approximating concrete behavior using continuum mechanics. To describe concrete materials, we need, in addition to the standard elastic description, a yield function and a way to describe the plastic behavior. In addition, concrete has other properties in tension than in compression.

Sammendrag

Betong er et viktig materiale ved bygging av militære anlegg. Hva skjer når disse anleggene blir utsatt for angrep fra prosjektiler? For å beregne dette trengs det en god forståelse av hvordan betongen oppfører seg. Empiriske og teoretiske modeller som estimerer penetrasjonsdybden til prosjektiler i betong bruker stort sett to parametere: trykkfasthet og tetthet. Dersom en skal simulere penetrasjon i betong numerisk, trengs en mer detaljert beskrivelse av betongen. Denne rapporten gir en oversikt over ulike betongmodeller.

Betong er et inhomogent materiale. Det består at sement, tilslag og armering. I litteraturen eksisterer det flere materialmodeller som beskriver betongen ved hjelp av kontinuumsmekanikk. I tillegg til elastiske parametere, trenger vi en flytekurve og en beskrivelse av hvordan betongen oppfører seg etter at flytegrensen er nådd. I tillegg har betongen ulike egenskaper i trykk og strekk.

Contents

1   Introduction

Concrete is an important material in building protective structures. To calculate what happens to these structures when exposed to impact loads, we need to have a good understanding of the material behavior. Empirical and theoretical models to estimate penetration depth, as discussed in Sjøl [1] and Teland and Sjøl [2], include only compressive strength and density. When performing a numerical simulation, a more detailed description is needed.

In this report, an overview over different material models for concrete is given.

Concrete is an inhomogeneous material, consisting of mortar, aggregate and in many cases reinforcement. In the literature, there exist several models approximating concrete behavior using continuum mechanics. To describe concrete materials, we need, in addition to the standard elastic description, a yield function and a way to describe the plastic behavior. In addition, concrete has different properties in tension than in compression.

2   Basic elasticity theory

In this chapter, a brief description of the elastic parameters and the relationship between them are described.

2.1   Stress tensor

A tensor is a quantity that is independent of coordinate system. A relationship on tensor form is therefore valid in all coordinate systems, which is very convenient for expressing physical laws. The stress tensor is denoted as

$$\boldsymbol{\sigma} = \begin{bmatrix} \sigma_x & \tau_{xy} & \tau_{xz} \\ \tau_{yx} & \sigma_y & \tau_{yz} \\ \tau_{zx} & \tau_{zy} & \sigma_z \end{bmatrix} \tag{2.1}$$

Note that the components of Equation (2.1) depend on the coordinate system used. If we change the coordinate system, the stress tensor components will have other values, but these will be related to the old components in a way which makes sure that the stress tensor itself is coordinate independent. From the components we can derive a set of stresses which are independent of the coordinate system. We call them principal stress, and denote them as σ_1, σ_2 and σ_3.

2.1.1 Principal stress

The principal stresses is defined as eigenvalues to the stress sensor, and is the solution of the characteristic equation

$$\sigma^3 + I_1\sigma^2 + I_2\sigma + I_3 = 0 \tag{2.2}$$

where I_1, I_2, I_3 are the stress invariants

$$\begin{aligned} I_1 &= \sigma_1 + \sigma_2 + \sigma_3 \\ I_2 &= \sigma_1\sigma_2 + \sigma_2\sigma_3 + \sigma_3\sigma_1 \\ I_3 &= \sigma_1\sigma_2\sigma_3 \end{aligned} \tag{2.3}$$

The characteristic equation has three real roots, $\sigma_1 > \sigma_2 > \sigma_3$.

2.1.2 Deviatoric stress tensor

The deviatoric stress s_{ij} is defined as

$$s_{ij} = \sigma_{ij} + \frac{1}{3}I_1 \tag{2.4}$$

And the deviatoric stress invariants are given by:

$$\begin{aligned} J_1 &= 0 \\ J_2 &= \frac{1}{3}I_1^2 - I_2 \\ J_3 &= \frac{2}{27}I_1^3 - \frac{1}{3}I_1 I_2 + I_3 \end{aligned} \tag{2.5}$$

The solution of the characteristic equations can be found by using the trigonometric relationship

$$\cos^3\theta - \frac{3}{4}\cos\theta - \frac{1}{4}\cos 3\theta = 0 \tag{2.6}$$

If we define

$$s = \rho\cos\theta \tag{2.7}$$

we get

$$\cos 3\theta - \frac{J_2}{\rho^2}\cos\theta - \frac{J_3}{\rho^3} = 0 \tag{2.8}$$

By comparing terms in Equation (2.6) and (2.8), we have [3]

$$\rho = \frac{2}{\sqrt{3}}\sqrt{J_2} \qquad \cos 3\theta = \frac{4\,J_3}{\rho^3} = \frac{3\sqrt{3}}{2}\frac{J_3}{J_2^{3/2}} \tag{2.9}$$

2.1.3   Octahedral stress

The octahedral stress plane is defines as a plane where the normal makes equal angels with each of the principal stresses. The normal and shear stress on the octahedral plane can be written as

$$\sigma_{oct} = (\sigma_1 + \sigma_2 + \sigma_3)/3 \qquad \tau_{oct} = \left(\frac{2}{3}J_2\right)^{1/2} \tag{2.10}$$

2.1.4   Equivalent stress

The equivalent stress σ_{eq} is defined as

$$\sigma_{eq} = \sqrt{3J_2} \tag{2.11}$$

2.2   Strain tensor

The strain tensor is defined in a similar way as the stress tensor, and is denoted as

$$\varepsilon = \begin{bmatrix} \varepsilon_{11} & \varepsilon_{12} & \varepsilon_{13} \\ \varepsilon_{21} & \varepsilon_{22} & \varepsilon_{23} \\ \varepsilon_{31} & \varepsilon_{32} & \varepsilon_{33} \end{bmatrix} \tag{2.12}$$

2.3 Stress-strain relationship

The relationship between stress and strain is found experimentally. For metals, this relationship is linear, and is described by Hooke's law. For concrete, however, there is a nonlinear relationship, and the stress-strain relationship in more complicated even in the elastic region.

2.3.1 Linear elastic models

Linear elastic models is the simplest model, but are unfortunately too simple to describe concrete materials well. Using Einstein's summation convention, a generalized Hooke's law can be written as

$$\sigma_{ij} = E_{ijkl}\varepsilon_{kl} \tag{2.13}$$

For homogenous and isotropic materials, the equation simplifies to $\sigma_{ij} = E\varepsilon_{ij}$.

2.3.2 Non-linear elastic models

Non-linear elastic models are often written on differential form:

$$\mathrm{d}\sigma_{ij} = E_{ijkl}\mathrm{d}\varepsilon_{kl} \tag{2.14}$$

where E_{ijkl} is no longer a constant, but a function of the strain tensor.

2.4 Haigh-Westegaard coordinates

The yield limit is the combination of stresses, strains etc for which the material stops behaving elastically. In some cases it can be visualized as a surface in principal stress space. A handsome way to visualize the yield stress, is to make a cross section through the hydrostatic axis, defined by $I_1 = 0$. This is called a pi-plane. For pressure dependent yield curves, which is used for concrete, it is convenient to use cylindrical coordinates, called (ρ, s, Θ), Haigh-Westegaard coordinates. The principal stress can be written in Haigh-Westegaard coordinates:

$$\begin{bmatrix} \sigma_1 \\ \sigma_2 \\ \sigma_3 \end{bmatrix} = \frac{1}{\sqrt{3}}\begin{bmatrix} \rho \\ \rho \\ \rho \end{bmatrix} + \sqrt{\frac{2}{3}}s\begin{bmatrix} \cos\theta \\ \cos(\theta - {}^{2\pi}/_3) \\ \cos(\theta + {}^{2\pi}/_3) \end{bmatrix} \tag{2.15}$$

where

$$\rho = I_1/\sqrt{3}$$
$$s = \sqrt{2J_2}$$
$$\cos 3\theta = \frac{3\sqrt{3}}{2} \frac{J_3}{J_2^{1,5}} \tag{2.16}$$

Θ is also called the Lode angle.

2.5 Yield criteria for homogenous materials

Here we list some popular yield criteria for homogenous materials. The Mises criterion is defined as

$$F(J_2) = J_2 - k^2 \tag{2.17}$$

And the Tresca criterion (maximum shear stress) is given by

$$F(\sigma_1, \sigma_2, \sigma_3) = \frac{1}{2}\max\{|\sigma_1 - \sigma_2|, |\sigma_2 - \sigma_3|, |\sigma_3 - \sigma_1|\} - k \tag{2.18}$$

Tresca's yield criterion can also be express using stress invariants, but this is too complicated to have any practical use. In Haigh-Westegaard coordinates, the von Mises and Tresca criterion becomes:

$$F(s) = s^2 - \frac{2}{3}Y$$
$$F(s, \theta) = \sqrt{2}s \sin\left(\theta + \frac{\pi}{3}\right) - \frac{Y}{2} \tag{2.19}$$

where Y is the uniaxial yield stress.

In the pi-plane, the von-Mises criterion is a circle, while Tresca's criterion is a hexagon. In Figure 2.1, the von Mises and Tresca's yield criterion is showed in the pi-plane and principal stress space, respectively.
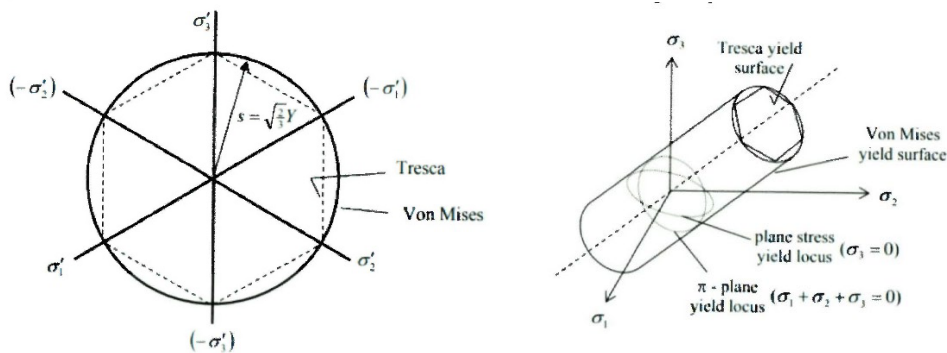
Figure 2.1   von Mises and Tresca yield criterium in the pi plane and principal stress space.

3   Constitutive models for concrete

The empirical and theoretical models studied in FFI-project 766 used only the compressive strength and density as material parameters. This is sufficient to estimate the penetration depth fairly well. However, if we are interested in more than the penetration depth, say the crack propagation, or the amount of spalling and scabbing, then a more advanced material model for concrete is needed. Several material models were studied in project 766.

The stress-strain relationship is found from material testing. There exist several methods of obtaining material parameters, both in the elastic and plastic region. An overview of constitutive models for concrete can be found in Babu et al (2005) [4]. Some test methods for obtaining the material parameters, are discussed in Teland and Svinsås (2003) [5].

4   Equation of state

For a linear elastic material, the complete behaviour is given by Hooke's law. If desired, we can transform Hooke's law into equations relating the stress deviations to strain deviations and pressure to density (Equation of state - EOS), but there is no need to do so. However, this is very convenient for describing materials that have reached the yield limit. Often the plastic behaviour is governed by completely independent plastic equations (for strain deviations) and Equations of state (for compression). Concrete is such a material, where it is necessary to supply

an EOS to describe the behaviour after reaching the elastic limit.

The simplest EOS is that the density remains constant (independent of pressure – a good approximation for water at low pressures). Such a material is said to be incompressible. However, concrete is not incompressible and requires a more complicated EOS. Some alternatives are described in this chapter.

4.1   Porous EOS

The porous EOS is defined as

$$P = K\eta \tag{4.1}$$

Where $\eta = 1 - \frac{\rho_0}{\rho}$ is the volumetric strain.

4.2   P-α EOS

The P-α model assumes that the internal energies and matrix material are identical. If the EOS for the matrix material can be written on the form

$$p = f(v, e) \tag{4.2}$$

where v is specific volume and e is internal energy, the EOS of the porous material can be written on the form

$$p = f(v/\alpha, e) \tag{4.3}$$

The P-α model is often used together with the RHT model.

4.3   Murnaghan EOS

The Murnaghan EOS is defined as

$$P = \frac{K}{\gamma}\left[\left(\frac{\rho}{\rho_0}\right)^{\gamma} - 1\right] \tag{4.4}$$

where $K = \rho_0 C_0^2$ is the bulk modulus of target material with C_0 = bulk sound speed. γ is related to the slope s of the linear Hugoniot relationship between the shock velocity and particle velocity [6].

$$\gamma = 4s - 1 \tag{4.5}$$

Note that Murnsghan's EOS is identical with the porous EOS for $\gamma = -1$.

5 Yield criteria for concrete

Most materials exposed to small loads will have small and elastic deformations. At some point, called the yield limit, the deformations will become plastic and permanent. The yield limit is a function of the stress tensor. By using the principal stresses or the stress invariants, the yield stress is independent of the coordinate system used. The yield stress can in general be written as

$$F(\sigma_1, \sigma_2, \sigma_3, \boldsymbol{n}, k) = 0 \qquad (5.1)$$

where **n** is the direction of the principal stresses, and k is the yield limit. To describe complex materials, such as concrete, several yield criteria have been suggested. They are all functions of the stress invariants, and have two, three, four or five parameters to describe the material. A review of these models can be found in Chen [3], and is listed in Table 5.1. All these models are pressure dependent. A brief discussion of some of these models are given in the next subsections.

Table 5.1   Yield crieria for concrete

Number of parameters	Model	Remarks
2	Drucker Prager Mohr Coloumb	"Extended" Mises "Extended" Tresca
3	Bresler-Pister William Warnke Lubliner	"Extended" Drucker-Prager
4	Menetray and William Mises Schleicher Hsieh-Ting-Chen Ottosen	
5	5 param. William Warnke	

5.1 Two parameter models

5.1.1 Mohr-Coulomb

The Mohr-Coulomb model was first expressed by Coulomb in 1773 as

$$|\tau| = c - \sigma_n tan\phi \tag{5.2}$$

where c is "cohesion" and ϕ is «angle of internal friction».

Note that the Mohr Coulomb model is reduced to Tresca's criterion setting $\phi = 0$ and c = k. The Mohr-Coulomb criterion can be expressed as a function of the principal stresses:

$$F(\sigma_1, \sigma_2, \sigma_3) = \sigma_1 - \sigma_3 - 2c \cos \phi + (\sigma_1 + \sigma_3) \sin \phi \tag{5.3}$$

Note that the Mohr Coulomb criterion is independent of the middle principal stress.

Abbo and Sloan [7] made a hyperbolic approximation to make the yield strength function smooth.

$$F = \sigma_m + \sqrt{\sigma^2 K^2(\theta) + a^2 \sin^2 \phi} - c \cos \phi \tag{5.4}$$

The parameter a can be adjusted to give a better approximation. This approximation is shown in Figure 5.1.
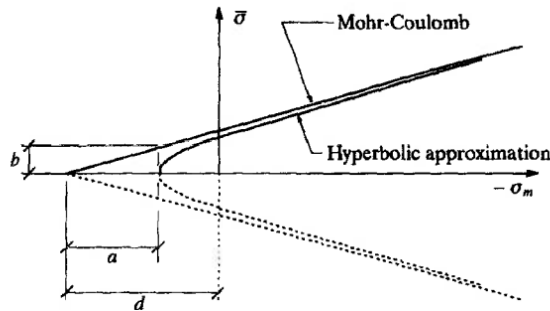
Figure 5.1   Hyperbolic approximation to the Mohr Coulomb criterion (from [7]).

The yield strength in Haigh-Westegaard coordinates becomes:

$$F(\rho, s, \theta) = \sqrt{2}\rho \sin \phi + \sqrt{3}s \sin \left(\theta + \frac{\pi}{3}\right) + s \cos \left(\theta + \frac{\pi}{3}\right) \sin \phi - \sqrt{6}c \cos \phi \tag{5.5}$$

The Mohr Coulomb model is an irregular hexagon in the pi-plane, and the meridians are straight lines. Figure 5.2 shows Drucker-Prager and Mohr-Coulomb in the principal stress space and the pi-plane.
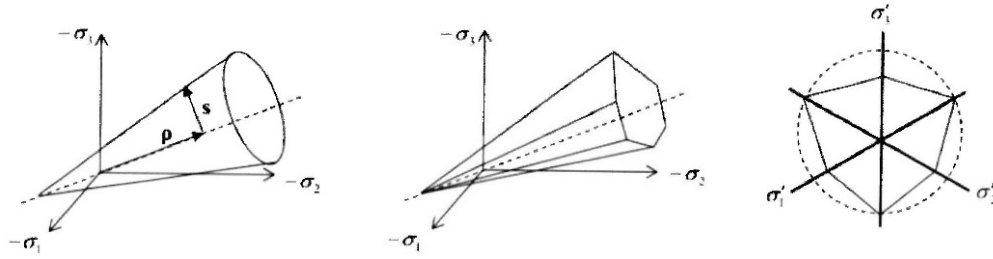
Figure 5.2   Drucker-Prager and Mohr-Coulomb criteria in principal stress space and pi-plane.

5.1.2 Drucker-Prager

$$F(I_1, J_2) = \alpha I_1 + \sqrt{J_2} - k = 0 \tag{5.6}$$

where α is a material constant. α = 0 gives the Mises criterion. In the pi plane, $I_1 = 0$, and «yield locus» becomes a circle. While the Mises criterion is a cylinder in the principal stress space, the Drucker-Prager criterion is a circular cone, as shown in Figure 5.2.

5.2 Three parameter models

The Drucker-Prager surface in the meridian plane is linear curves, and the cross sections in the deviatoric plane (pi-plane) are circles. Experiments shows that the plot in the meridian space are curved, and the cross sections in the pi-planes are non-circular. To incorporate this fact, another parameter is needed to describe the yield surface. In some models, an elliptical function with the Lode angle is included. This elliptical function is defined as

$$r(\theta, e) = \frac{4(1 - e^2)\cos^2\theta + (2e - 1)^2}{2(1 - e^2)\cos^2\theta + (2e - 1)\sqrt{4(1 - e^2)\cos^2\theta + 5e^2 - 4e}} \tag{5.7}$$

5.2.1 Bresler-Pister

The Bresler-Pister model assumes a parabolic relationship, and can be expressed using octahedral stress

$$F = \frac{\tau_{oct}}{f_c} = a - b\,\frac{\sigma_{oct}}{f_c} + c\left(\frac{\sigma_{oct}}{f_c}\right)^2 \tag{5.8}$$

Plasticity model for concrete based on Bresler-Pister can be found in Dede and Ayvaz (2010) [8].

5.2.2   William-Warnke

William and Warnke (1975) [9] defined the following 3 parameter model

$$F = \left[\sqrt{1{,}5}\frac{\rho}{f_c}\right] + m\left[\frac{\rho}{\sqrt{6}f_c}r(\theta, e) + \frac{\xi}{\sqrt{3}f_c}\right] \tag{5.9}$$

Where ξ is hydrostatic stress invariant, ρ is deviatoric stress invariant and θ is deviatoric polar angle. This model has straight meridians and non-circular cross sections. In Section *, this model is extended with two additional parameters in order to model the materials for high pressures in compression.

5.2.3   Lubliner yield criterion

The Lubliner yield criterion is originally a four parameter model, but the yield criterion in uniaxial compression reduces the yield surface to

$$F = \sqrt{3J_2} + \alpha I_1 + \beta\langle\sigma_{max}\rangle - \gamma\langle-\sigma_{max}\rangle - (1 - \alpha)c \tag{5.10}$$

where

$$\langle x \rangle = (|x| + x)/2 \tag{5.11}$$

This model is used in Cicekli (2006,2007) [10, 11] and in In Zhang and Li (2012) [12].

5.3   Four parameter models

5.3.1   Ottosen yield surface

Ottosen (1977) [13] developed a four-parameter model. This model contains all stress invariants, and is valid for all stress combinations.

$$F = a\frac{J_2}{f_c^2} + \lambda\frac{\sqrt{J_2}}{f_c} + b\frac{I_1}{f_c} - 1 \tag{5.12}$$

Where a and b are parameters, and λ is given by

$$\lambda = \begin{cases} K_1 \cos\left[\dfrac{1}{3}\arccos(K_2 \cos 3\theta)\right] & \cos 3\theta \geq 0 \\[2mm] K_1 \cos\left[\dfrac{\pi}{3} - \dfrac{1}{3}\arccos(-K_2 \cos 3\theta)\right] & \cos 3\theta \leq 0 \end{cases} \tag{5.13}$$

The factors K_1 (size factor) and K_2 (shape factor) are between 0 and 1. In Zhang et al (2020) [14], a constitutive model based on Ottosen yield criterion was developed. The plastic potential is

$$Q = \frac{a}{k^2 q^{0,5}} \frac{J_2}{f_c^2} + \left(1 + \frac{k}{q^2}\right)\left(\lambda \frac{\sqrt{J_2}}{f_c} + F_c b \frac{I_1}{f_c}\right) - d = 0 \tag{5.14}$$

5.3.2   Menetrey and William (1995)

This is a modification of the Hoek and Brown [15] model, see for example Radoslav (2017) [16]

$$F = \left(\sqrt{1,5}\,\frac{\rho}{k(\kappa)f_c}\right)^2 + m\left(\frac{\rho}{\sqrt{6}\,k(\kappa)f_c}\,r(\theta,e) + \frac{\xi}{\sqrt{3}\,k(\kappa)f_c}\right) - c(\kappa) \tag{5.15}$$

where

$$m = 3\,\frac{(k(\kappa)f_c)^2 - (\lambda_t f_t)^2}{k(\kappa)f_c \lambda_t f_t}\,\frac{e}{e+1} \tag{5.16}$$

In this model, m is a parameter equivalent to cohesion, r is an elliptical function, e is the eccentricity of the elliptical function (between 0,5 and 1,0), and λ_t is a scaling parameter of the M-W-3 surface (greater than 1,0). k is a strengthening parameter at plasticization moment (close to 1,0).
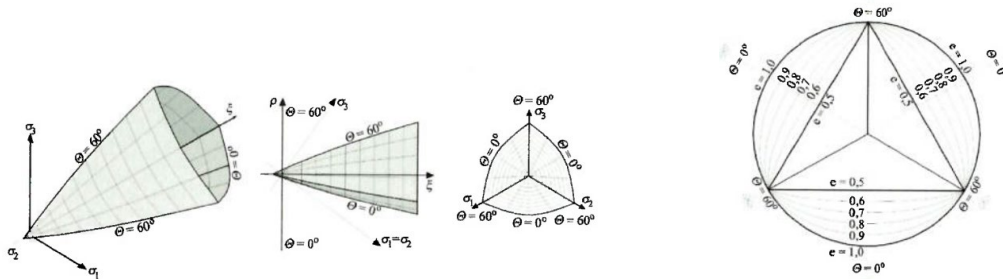
Figure 5.3   Menetrey and William model.

FFI-RAPPORT 23/00669

5.3.3 Mises Schleicher

The Mises Schleicher crtiterion is defined as (see for example Shen et al (2015) [17])

$$F = \sigma_{eq}^2 + 3\alpha\sigma_0\sigma_m - \sigma_0^2 \qquad (5.17)$$

where

$$\alpha = \frac{\sigma_c - \sigma_T}{\sqrt{\sigma_c\sigma_T}}$$
$$\sigma_0 = \sqrt{\sigma_c\sigma_T} \qquad (5.18)$$

In Durban et al (2010) [18], the Mises Schleicher criterion is used. An exact solution can be found in Monchiet and Kondo (2012) [19].

5.3.4 Hsieh-Ting-Chen criterion (1979)

The Hsieh-Ting-Chen criterion is a four parameter model, which is a combination of Rankine, Mises and Drucker-Prager models.

$$F = a\frac{J_2}{f_c'^2} + b\frac{\sqrt{J_2}}{f_c'} + c\frac{\sigma_1}{f_c'} + d\frac{I_1}{f_c'} - 1 \qquad (5.19)$$

- If a = c = 0, we get the Drucker-Prager criterion.

- If a = c = d = 0, we get the von Mises criterion.

- If a = b = d = 0, and c = fc/ft, we get the Rankine criterion.

Plasticity model for concrete based on Hsieh-Ting-Chen criterion can be found in Dede and Ayvaz (2010) [20]. In Haigh-Westegaard coordinates, we get

$$F = \sqrt{2J_2} - \frac{1}{2a}\left[-(b\cos\theta + c) + \sqrt{(b\cos\theta + c)^2 - 4a\left(\sqrt{3}d\frac{I_1}{3} - 1\right)}\right] \qquad (5.20)$$

5.3.5 Reimann criterion

Reimann (1965) suggested a four parameter hyperbolic criterion

$$\frac{\xi}{f_c'} = a \left(\frac{r_c}{f_c'} \right)^2 + b \frac{r_c}{f_c'} + c \qquad (5.21)$$

According to Chen [3], this criterion works best in compression, and will not be analyzed further in this report.

5.4 Five parameter model

A refined William Warnke model, giving a general expression for both the compressive and tensile meridian, is defined as

$$\begin{aligned}
\frac{\tau_{mt}}{f_c} &= \frac{r_t}{\sqrt{5} f_c} = a_0 + a_1 \frac{\sigma_m}{f_c} + a_2 \left(\frac{\sigma_m}{f_c} \right)^2 \\
\frac{\tau_{mc}}{f_c} &= \frac{r_c}{\sqrt{5} f_c} = b_0 + b_1 \frac{\sigma_m}{f_c} + b_2 \left(\frac{\sigma_m}{f_c} \right)^2
\end{aligned} \qquad (5.22)$$

We have here six unknown parameters, but if we in addition specify that these meridians both intersect the hydrostatic axis at $\sigma_{m0}/f_c = \rho$, the number of parameters is reduced to five.

5.5 Comparison yield models

Figure 5.4 shows schematically some of these models (from Riedel et al [21]).
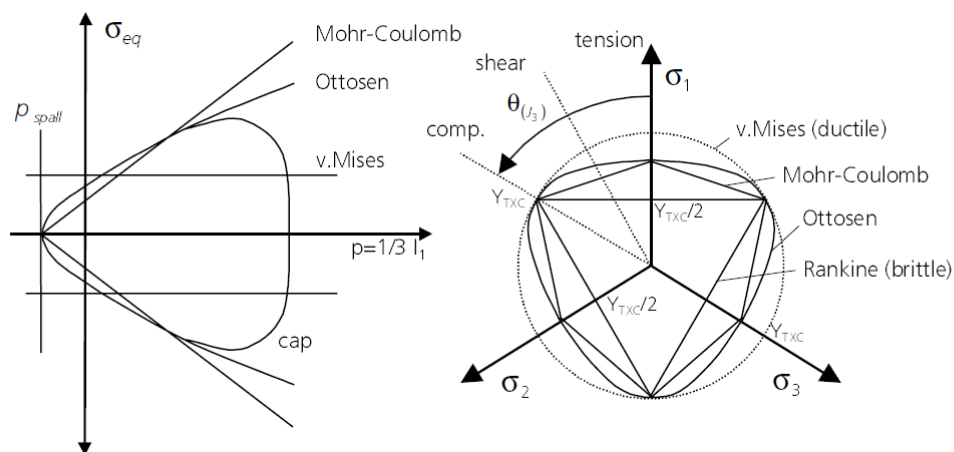
Figure 5.4 Different yield models for concrete (from Riedel et al [21])

6 Plasticity models

Plasticity models for reinforced concrete are discussed in Chen (1982) [3]. The strain increment can be decomposed into an elastic part and a plastic part

$$d\epsilon_{ij} = d\epsilon_{ij}^e + d\epsilon_{ij}^p \qquad (6.1)$$

A plasticity model must contain

- Yield surface (described in the previous sections)

- Flow rule

- Hardening rule

In the elastic region, the governing equations, with appropriate boundary conditions, have well defined and unique solutions. In a plastic material, this may not be obvious. To assure uniqueness and stability of the solution, the yield surface must satisfy certain (physical) requirements:

- Smoothness

- Convex

- Non-circular deviatoric section

Table 6.1   Some plasticity models with non-associative flow rule described in Babu et al [4].

Model	Yield surface	Hardening law
Grassl (2002)	Menetrey & William	
Imran et al (2001)	Hsieh-Ting-Chen	Isotropic
Feenstra et al (1996)	Drucker-Prager	
Onate et al (1988)	Modified MC	
Vermeer et al (1984)	Mohr Coloumb	

6.1 Flow rule

A flow rule is in general defined as

$$d\varepsilon_{ij}^{p} = d\lambda \frac{\partial Q}{\partial \sigma_{ij}} \qquad (6.2)$$

where $d\lambda$ is a nonnegative scalar and Q is a plastic potential function. When Q is equal to the yield function F, we have an associated flow rule. For concrete, however, experimental data [22-24] indicate that an associated flow rule does not give a correct description.

6.1.1 Drucker stability

Drucker defined a stable material to satisfy the following statements:

- Positive work by external agency during the application of the loads

- The net work performed by the external agency over a stress cycle is nonnegative

Equation (6.2) implies that the plastic flow vector $d\varepsilon_{ij}^{p}$ is perpendicular to the plastic potential surface (see Chen [3]). Another implication is that the yield surface must be convex.

6.1.2 Shear dilatancy

Shear dilatancy is a phenomenon characterized by volume change associated with shear distortion of the material. Several experimental data from the literature shows that concrete materials have this property. In the next sections, we first explain the property of an elastic perfectly plastic material.

6.1.3 Prandtl-Reuss material

A Prandtl-Reuss material is an elastic perfect plastic material. It follows from the definition that all volume change is elastic. Hence, we have no plastic strain.

6.1.4 Drucker-Prager based potential

A Drucker-Prager based potential can be written on the form

$$Q(\sigma_{ij}, \alpha) = \alpha I_1 + \sqrt{J_2} + Constant \qquad (6.3)$$

where α can be found from uniaxial compression test:

$$\alpha = \frac{1}{\sqrt{3\left[1 - \dfrac{\varepsilon^p}{\varepsilon_v^p}\right]}} \tag{6.4}$$

ε_v^p is volumetric part of the plastic strain. It can be shown from Equation (6.4) that the plastic rate of cubical dilatation is

$$d\varepsilon_{ij}^p = 3\alpha \, d\lambda \tag{6.5}$$

This means that we have an increase in volume, which is due to the face that the yield function is pressure dependent.

6.1.5   Mohr Coulomb based potential

A Mohr Coulomb based potential can be written as

$$Q = \frac{I_1}{3}\sin\psi + \sqrt{J_2}\left[\cos\theta - \frac{\sin\theta\sin\psi}{\sqrt{3}}\right] \tag{6.6}$$

where ψ is the angle of dilatancy (found experimentally). This model is among others used in Vermeer and de Borst (1984) [23].

6.2   Hardening rule

The perfectly plastic model described in Section 6.1.3 has a fixed failure surface in the stress space. This is not true for most materials, and we need a way to describe the "motion" of the yield surface during plastic flow. This is called a hardening rule. We have two different hardening rules, and a combination of these.

- Isotropic hardening is a uniform expansion of yield surface.

- Kinematic hardening is a translation of the yield surface as a rigid body in stress space.

- Mixed hardening is a combination of isotropic and kinematic hardening.

$$d\epsilon^p = d\epsilon^{pi} + d\epsilon^{pk} = M \, d\epsilon^p + (1 - M) \, d\epsilon^p \tag{6.7}$$

where M is a mixed hardening parameter between 0 and 1.

6.3   CAP models

The yield surfaces described in Chapter 5 have no yield along the hydrostatic axis. To control the dilatation of soils, a "cap function" was introduced. The simplest way of doing this, is to introduce a plane cap, but this may introduce discontinuities in the derivatives.

6.3.1   Drucker Prager with cap

6.3.1.1   Plane cap

The loading function can be separated in three parts:

- A yield surface for loading and failure $F_1 = \alpha I_1 + \sqrt{J_2} - \kappa(\epsilon_p) = 0$

- A compression plane cap surface $F_c = I_1 - x(\epsilon_{kk}^p) = 0$

- A tension cutoff limit plane $F_t = I_1 - T = 0$

This is schematically shown in Figure 6.1.
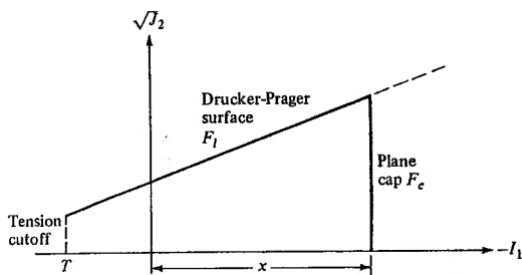
Figure 6.1   Drucker Prager with plane cap

6.3.1.2   Elliptic cap

The elliptic cap model is defined by using a quarter of an ellipse for the strain hardening cap function:

$$F_c = (I_1 - l)^2 + R^2 J_2 - (x - l)^2 = 0 \qquad (6.8)$$

Where l is the value of I_1 at the center of the cap and R is the ratio of the major to minor axis of the elliptic cap (may be a function of l). This is shown in Figure 6.2.
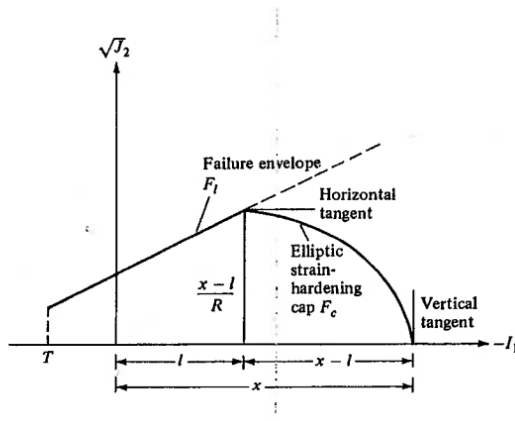
Figure 6.2   Drucker Prager with elliptical cap

6.3.2   LS DYNA

In LS DYNA, there is an inbuilt continuous surface cap model (CSCM), see the user's manual [25]

$$F = J_2 - \Re^2(J_3)F_f^2(J_1)F_c(J_1, \kappa) \tag{6.9}$$

where $\Re$ is Rubin three invariant reduction factor, F_f is the shear failure surface and F_c is the hardening cap. The Rubin reduction factor is illustrated in Figure 6.3, where a two-invariant circle in the pi-plane is reduced to an (in general) irregular hexagon.
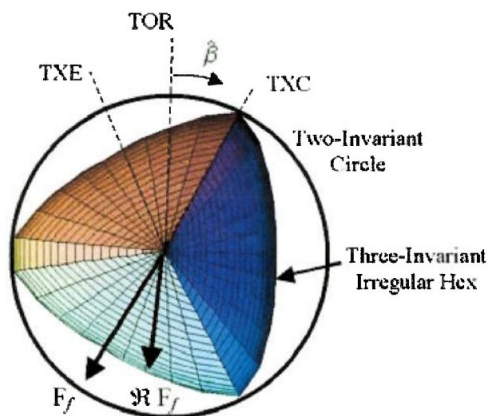
Figure 6.3   Illustration of the Rubin reduction factor in the pi-plase, from the LS-DYNA manual).

The Rubin reduction factor is (see LS-DYNA manual)

$$\Re = \frac{-b_1 + \sqrt{b_1^2 - 4b_2 b_0}}{2b_2} \tag{6.10}$$

where

$$\begin{aligned}
b_2 &= \left(\cos\hat{\beta} - a\sin\hat{\beta}\right)^2 + b\sin^2\hat{\beta} \\
b_1 &= a\left(\cos\hat{\beta} - a\sin\hat{\beta}\right) \\
b_0 &= -(3 + b - a^2)/4
\end{aligned} \tag{6.11}$$

$$\begin{aligned}
b &= (2\,Q_1 + a)^2 - 3 \\
a &= \frac{-a_1 + \sqrt{a_1^2 - 4a_2 a_0}}{2a_2}
\end{aligned} \tag{6.12}$$

$$\begin{aligned}
a_2 &= Q_2 \\
a_1 &= \sqrt{3}\,Q_2 + 2\,Q_1(Q_2 - 1) \\
a_0 &= 2\,Q_1^2\,(Q_2 - 1)
\end{aligned} \tag{6.13}$$

The shear failure surface F_f is given by

$$F_f(J_1) = \alpha - \lambda\exp(-\beta J_1) + \theta J_1 \tag{6.14}$$

The Rubin reduction formulation is more flexible in fitting experimental data than the William-Warnke model. From the LS DYNA model, four example fits are listed:

- Most general fit

    o 8 input parameters

    o $Q_1 = \alpha_1 - \lambda_1\exp(-\beta_1 J_1) + \theta_1 J_1$ $\quad Q_2 = \alpha_2 - \lambda_2\exp(-\beta_2 J_1) + \theta_2 J_1$

- Mohr Coloumb fit

    o Straight lines between TXE and TXC

    o $Q_1 = \frac{\sqrt{3}\,Q_2}{1 + Q_2}$ and $Q_2 = \frac{3 - \sin\phi}{3 + \sin\phi}$

- Two parameter fit

    o Input α_1 and α_2. All other Rubin parameters are zero.

- William Warnke fit

FFI-RAPPORT 23/00669

○ Select Q_2 as a constant or as a function of pressure

○ $Q_1 = \dfrac{\sqrt{3}\ (1-Q_2^2)+(2Q_2-1)\sqrt{3\ (1-Q_2^2)+5\ Q_2^2-4\ Q_2}}{3\ (1-Q_2^2)+(1-2Q_2)^2}$

The hardening cap F_c is given by

$$F_c = 1 - \frac{[J_1 - L(\kappa)][|J_1 - L(\kappa)| + J_1 - L(\kappa)]}{2[X(\kappa) - L(\kappa)]} \tag{6.15}$$

This model has also been used in Saini et al (2021) [26] for low velocity impact on high performance fiber reinforced concrete.

7   RHT

Riedel et al [21] developed a rather complicated model to describe the damage curve for concrete. The yield surface is defined as

$$F = \sqrt{3J_2} - Y_{TXC}F_{CAP}R_3F_{RATE} \tag{7.1}$$

Where

$$Y_{TXC}^* = A_{fail} + B_{fail}\big[p^* - \big(p_{spall}^* F_{RATE}\big)\big]^{N_{fail}} \tag{7.2}$$

$$F_{RATE} = \begin{cases} 1 + R_1\, log\, \dfrac{\dot{\varepsilon}}{\dot{\varepsilon}_0} & \dot{\varepsilon} < \dot{\varepsilon}_{limit} \\[2mm] 1 + R_2\, log\, \dfrac{\dot{\varepsilon}}{\dot{\varepsilon}_0} & \dot{\varepsilon} > \dot{\varepsilon}_{limit} \end{cases} \tag{7.3}$$

$$R_3(\theta) = \frac{2(1-Q_2^2)\cos^2\theta + (2Q_2-1)\sqrt{4(1-Q_2^2)\cos^2\theta + 5Q_2^2 - 4Q_2}}{4(1-Q_2^2)\cos^2\theta + (1-2Q_2)^2} \tag{7.4}$$

Where Q_2 is a parameter between 0,5 and 1,0.

$$F_{CAP} = \begin{cases} 1 & p \le p_u \\ \sqrt{1 - \left(\dfrac{p - p_u}{p_0 - p_u}\right)^2} & p_u \le p \le p_0 \\ 0 & p_0 \le p \end{cases} \tag{7.5}$$

where Y_{TXC} adjust for triaxial compression, F_{CAP} defines the cap-model for high hydrostatic pressure, R_3 reduce the strength of concrete after damage and F_{RATE} adjust for strain rate effects. This model uses many parameters to describe the concrete, and may be difficult to apply. However, it was widely used around year 2000 and was implemented in the hydrocode Autodyn, see for example Hansson et al (2002) [27], and LS-DYNA. In Heckötter and Sievers (2017) [28], the implementation in these hydrocodes are compared. The main difference in these implementations, is how the initial parameters in the P-α EOS model are defined. In AUTODYN, the initial densities for the porous and matrix materials are given. In LS-DYNA, the initial porosity is defined.

8 K & C (Karagozian & Case)

The K&C model was developed in 1994, and later modified by several researchers. A summary of the model, and description of the parameters can for instance be found in Malvar et al [29]. This model was widely used by FOI around year 2000. Three independant yield surfaces are defined, «yield», «failure» and «maximum residual strength». All these surfaces are on trhe form

$$F_i = a_{0i} + \frac{P}{a_{1i} + a_{2i}P} \tag{8.1}$$

There is a total of 9 parameters a_{ki} to be determined. In Magallanes et al (2017) [30] and Kong et al (2017) [31], some recent improvements of the K&C model is presented.

In Saini et al (2021) [26], the K&C model is studied for low impact velocities on ultrahigh performance fiber reinforced concrete, and compared to the CSC (continuous surface cap) model.

9 Holmquist Johnson Cook (HJC)

The first version of the HJC model, was published by Johnson and Cook in the mid 1980s. It was originally constructed to describe metals when exposed to loads resulting in high strain rates. This model was later modified to describe concrete.

9.1 Johnson Cook (1983)

Johnson and Cook (1983) [32] developed a constitutive model for metals subjected to large strains, high strain rates and high temperatures. The von Mises flow stress is expressed as

$$\sigma = [A + B\varepsilon^n][1 + C \ln \dot{\varepsilon}^*][1 - T^{*m}] \qquad (9.1)$$

where ε is the equivalent plastic strain.

9.2 HJC (1993)

In the International Symposium on Ballistics in 1993, Holmquist, Johnson and Cook [33] presented a material model for concrete. In this paper, numerical simulations of experiments in Hanchak et al [34] is performed to verify the model.

The equivalent stress is in [33] given by

$$\sigma_{eq} = \sigma_c * min\left[sfmax, \left(A(1-D) + B\left(\frac{p}{\sigma_c}\right)^N\right) * \left(1 + Cln\left(\frac{\dot{\varepsilon}}{\dot{\varepsilon}_0}\right)\right)\right] \qquad (9.2)$$

where $p = 1/3I_1$. This is schematically shown in Figur 10.1. The parameters *A, B, C, N* and *Sfmax* is found from material testing, as described in [33]. The yield stress is given by

$$F = \sqrt{3J_2} - \sigma_c * min\left[sfmax, \left(A(1-D) + B\left(\frac{p}{\sigma_c}\right)^N\right) * \left(1 + Cln\left(\frac{\dot{\varepsilon}}{\dot{\varepsilon}_0}\right)\right)\right] \qquad (9.3)$$
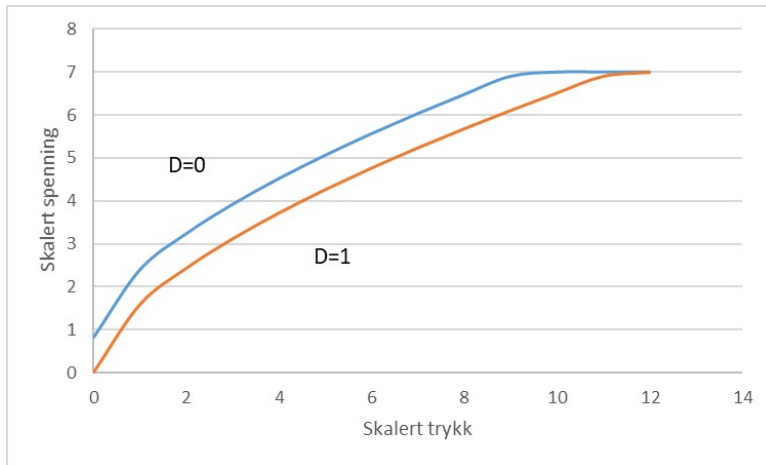
Figure 9.1   The yield stress.

The damage parameter D is defined as

$$D = \sum \frac{\Delta \varepsilon_p + \Delta \mu_p}{\varepsilon_p^f + \mu_p^f} \tag{9.4}$$

where the denominator is given by

$$\varepsilon_p^f + \mu_p^f = D_1(P + T)^{D_2} \tag{9.5}$$

When the concrete is crushed, the pressure will change. This is done in the following way:

$$P = K_1\bar{\mu} + K_2\bar{\mu}^2 + K_3\bar{\mu}^3 \tag{9.6}$$

where

$$\bar{\mu} = \frac{\mu - \mu_{lock}}{1 + \mu_{lock}} \tag{9.7}$$

μ_{lock} is different for different concrete types.
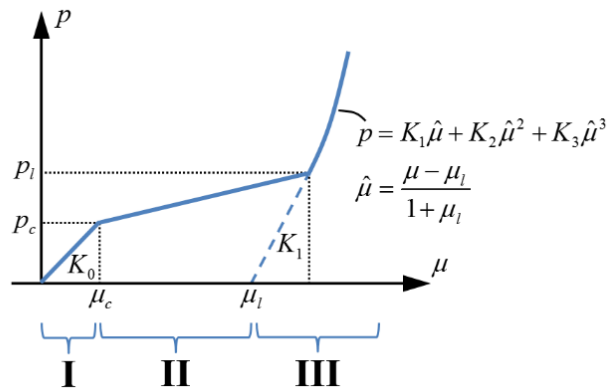
Figure 9.2   Pressure as a function of volumetric strain.

The HJC model has many parameters, which should be determined from material tests of the actual concrete. I Table 10.1, all parameters are described, and the values are taken from [33].

Tabell 9.1   Material parameters in the HJC model for 48 MPa concrete [33].

Strength		Damage		Pressure	
A	0,79	D_1	0,04	P_{crush}	0,016 GPa
B	1,6	D_2	1,0	μ_{crush}	0,001
N	0,61	EFMIN	0,01	K_1	85 GPa
C	0,007			K_2	-171 GPa
σ_c	48 MPa			K_3	208 GPa
Smax	7			P_{lock}	0,80 GPa
Shear modulus (G)	14,86 GPa			μ_{lock}	0,10
				T	0,004 GPa

This model is used in [33] to simulate perforation of a 25,4 mm projectile with impact velocity 400 m/s in a 48 MPa concrete slab. In Sjøl (2020), this simulation was repeated using the hydrocode Impetus Afea.

9.2.1 Polanco-Loria et al (2008)

Polanco-Loria et al (2008) [35] modified the HJC model in the following way:

$$F = \sigma_{eq} - B\big(P + T(1-D)\big)^N * \left(1 + \left(\frac{\dot{\varepsilon}}{\dot{\varepsilon}_0}\right)\right)^C * R(\theta, e) \tag{9.8}$$
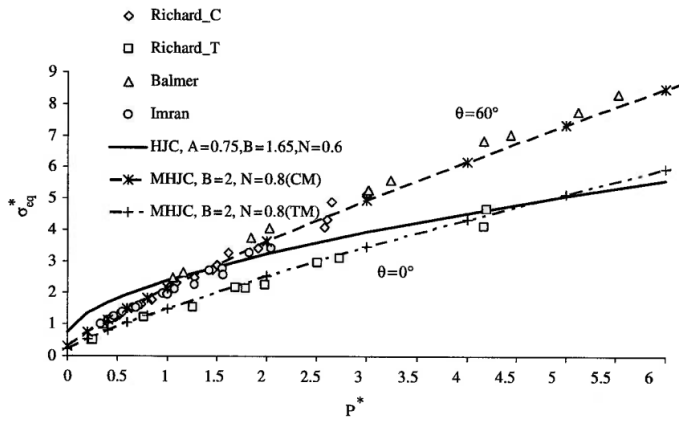
Figure 10.3 Equivalent stress as a function of normalized pressure. Comparison of HJC, MHJC and experiments. Figure taken from [35].

9.2.2 Islam et al (2013)

In Islam et al (2013) [36], the HJC model is modified. The numerical simulations is also compared to the experiments in Hanchak et al [34]. The yield strength in the modified HJC model is

$$F = \sqrt{3J_2} - \sigma_c * \left(A(1-D) + B\left(\frac{p}{\sigma_c}\right)^N\right) * C\left(\frac{\dot{\varepsilon}}{\dot{\varepsilon}_0}\right)^{\frac{1}{3}} \tag{9.9}$$

Compared to the original HJC model, there are two differencies. First, there is no maximum value of the equivalent stress. In addition, there is a slightly different way of including strain rate effects. The parameters describing the strain rate effects (C and $\dot{\varepsilon}_0$) are different in compression and tension.

9.2.3 Kong et al (2016)

Kong et al (2016) [37] cratering and scabbing modified HJC material model. In order to obtain a continuous yield surface for all pressure values, the following is proposed:

$$\sigma_{eq} = \sqrt{3J_2}$$

$$
= \begin{cases}
3[p + T\,(1 - D_t)]r' & p < 0 \\[2mm]
\left[3T\,(1 - D_t) - \dfrac{9pT\,(1 - D_t)}{f_c\,(1 - D_c)} + 3p\right]r' & 0 \le p \le f_c(1 - D_c)/3 \\[2mm]
\left[3p\left(1 - \dfrac{3T}{f_c}\right) + 3\,(1 - D_c)\,T\right]r' & f_c(1 - D_c)/3 \le p \le f_c/3 \\[2mm]
\left[f_c - 3TD_c + Bf_c\left(\dfrac{p}{f_c} - \dfrac{1}{3}\right)^N\right]r' & p > f_c/3
\end{cases}
\qquad (9.10)
$$

In addition to the parameters defined in the original HJC-model, we have D_t (cumulative tensile damage) and r', which is defined in Equation (5.7). The tensile failure D_t is based on the work in Weerheijm et al (2007) [38]

$$
D_t = \left(1 + \left(c_1 \frac{\bar{\varepsilon}_p}{\varepsilon_{frac}}\right)^3\right)\exp\left(-c_2 \frac{\bar{\varepsilon}_p}{\varepsilon_{frac}}\right) - \frac{\bar{\varepsilon}_p}{\varepsilon_{frac}}(1 + c_1^3)\exp(-c_2)
\qquad (9.11)
$$

Here, we have $\bar{\varepsilon}_p$ (effective plastic strain), ε_{frac} (fracture strain) and two constants c_1=3 and c_2 = 6,93 (from Kong et al (2016)).

10   Material models calibrated for blast loading

The yield curve in MAT_CONCRETE_2018 in Impetus is defined by

$$
\sigma_y =
\begin{cases}
0 & p < p_s \\[2mm]
\eta(p - p_s) & p_s < p < \xi p_c \\[2mm]
\eta(p - p_s)\sqrt{1 - \dfrac{1 - p/p_c}{1 - \xi}} & \xi p_c < p < p_c
\end{cases}
\qquad (10.1)
$$

This is shown graphically in Figure 10.1. Note that this material model is an associated flow model at the cap (for high hydrostatic pressure).
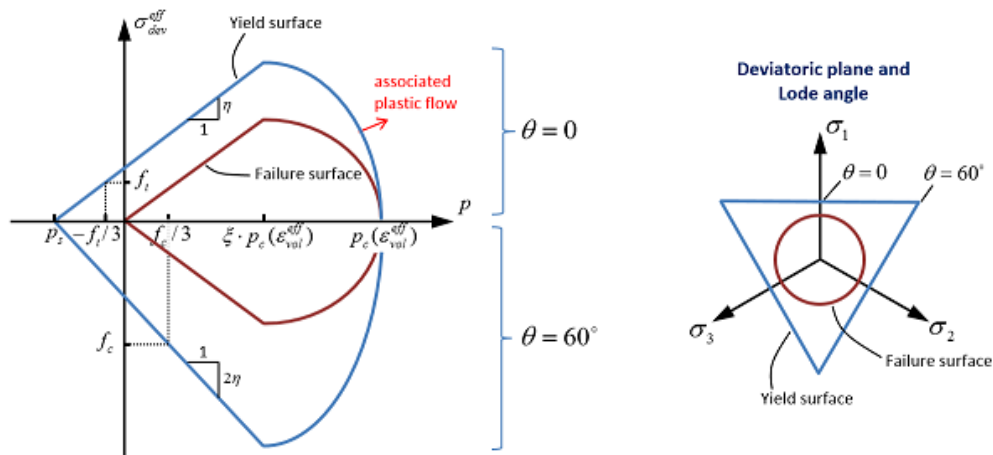
Figure 10.1 Damage model for MAT_CONCRETE_2018. The figure is taken from the Impetus manual [39]

In Impetus, the material parameters for MAT_CONCRETE_2018 are defined as:

```
*MAT_CONCRETE_2018
"Optional title"
mid, ρ, G
K₀, K_L, p₀, p_L, ε_L, n, f_t, f_c
r_f, r_e, ε_t, ε_c, c, cdec, ξ, bulk
KIc
```

In Table 10.1, these parameters are described.

Table 10.1   Parameters used in MAT_CONCRETE_2018.

Parameter	Description
mid	Material ID-number
ρ	Density
G	Shear modulus
K_0	Initial bulk modulus
K_L	Bulk modulus at full compaction
P_0	Hydrostatic pressure at "crush limit"

P_L og ε_L	Hydrostatic pressure og volumetric strain at full compaction
f_t og f_c	Uniaxial tensile and compressive strength
r_f og r_e	Strain rate parameters
ε_t	Uniaxial «failure tensile strain»
ε_c	Volumetric failure crushing strain
C og cdec	Parameters describing the viscosity of the material
ξ	Parameter controlling the shape of the yield surface
Bulk	0: No bulk ; 1: Bulking activated
KIC	Fracture toughness

11   Kong-Fang model

Kong et al (2018) [40] published a new model based on the best features of HJC, RHT and K&C models. This was later modified in 2020 by Zhang et al [41]. First, we recapture the shortcomings of the three models before we introduce the new model.

HJC has three shortcomings:

- In tension, HJC uses elastic perfect plastic model, which is too simple

- Only two stress invariants are used, which cannot capture the transition from triangular shape (low pressure) to circular shape (high pressure)

- J_2 flow rule is adopted, shear dilatation behavior cannot be reproduced

RHT has shortcomings

- Linear crack softening – too simple

- Use J_2 flow rule, which means that shear dilatation behavior cannot be captured

K& C has shortcomings

- Not well suited for high pressures, i e for projectile impact and contact blast loadings

- Dynamic tensile behavior is not consistent with experiments

- Tensile failure criterion is not available

The new Kong and Fang model include the advantages and discards the disadvantages of the HJC, RHT and K&C models.

11.1 Three invariant failure surface

The maximum and residual strength surface are defined as

$$
\sigma_m = \begin{cases} 3[P/(1-D)+T] & P \leq 0 \\ 1{,}5(P+T)/\psi & 0 < P \leq f_c/3 \\ f_c + \dfrac{P - f_c/3}{a_1 + a_2 P} & P > f_c/3 \end{cases} \tag{11.1}
$$

$$
\sigma_r = \begin{cases} 0 & P \leq 0 \\ \dfrac{P}{a_1 + a_2 P} & P > 0 \end{cases} \tag{11.2}
$$

Where

$$
\psi(P) = \begin{cases} 0{,}5 & P \leq 0 \\ 0{,}5 + 1{,}5\,T/f_c & P = \dfrac{f_c}{3} \\ 1{,}15/[1 + 1{,}3/(3a_1 + 2{,}3a_2 f_c)] & P = \dfrac{2{,}3 f_c}{3} \\ 0{,}753 & P = 3 f_c \\ 1 & P \geq 8{,}45 f_c \end{cases} \tag{11.3}
$$

For pressure between the points defined in Equation (11.4), linear interpolation is used. The maximum strength surface as a function of pressure is shown in Figure 11.1 for HJC, RHT, K&C compared to the Kong and Fang model and experiments from the literature. We see that, especially for high pressures, the Kong and Fang model is in better agreement with the experiments.
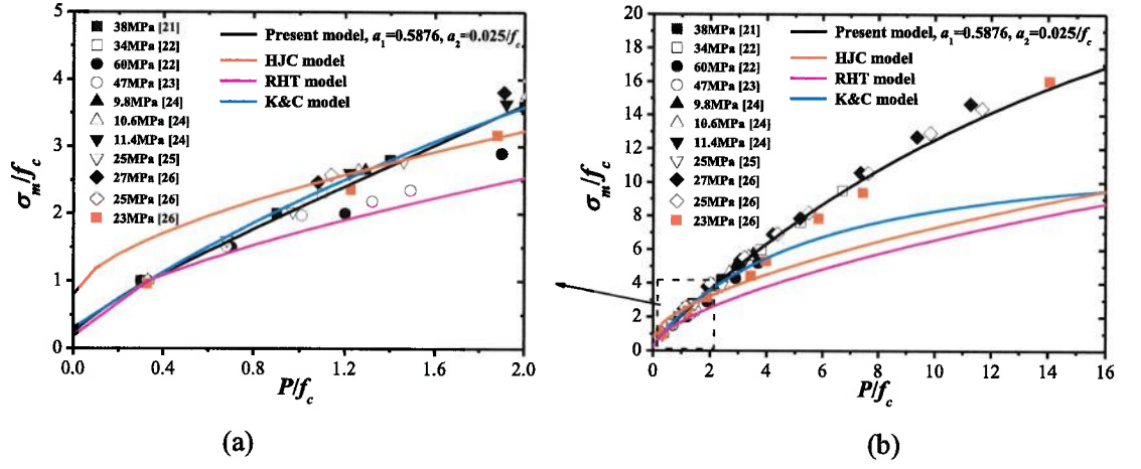
Figure 11.1 Maximum strength surface

Current failure surface:

$$Y(\sigma_{ij}, D) = \sqrt{3J_2} = r'[D(\sigma_r - \sigma_m) + \sigma_m] \tag{11.4}$$

Where

$$r'(\theta, \psi) = \frac{2(1-\psi^2)\cos\theta + (2\psi-1)\sqrt{4(1-\psi^2)\cos^2\theta + 5\psi^2 - 4\psi}}{4(1-\psi^2)\cos^2\theta + (1-2\psi)^2} \tag{11.5}$$

and θ is the Lode angle, see Chapter 2 for definition. Strain rate effects are taken care of by using a "Dynamic Increase Factor" (DIF - r_f):

$$Y = r_f Y(P/r_f) \tag{11.6}$$

r_f is defined different in compression and tension. The following expressions are found experimentally:

$$(r_f)_t = \{[\tanh(\log(\dot{\epsilon}/\dot{\epsilon}_0) - W_x)S](F_m/W_y - 1) + 1\}W_y$$
$$(r_f)_c = ((r_f)_t - 1)(T/f_c) + 1 \tag{11.7}$$

In Kong et al (2018), the reference strain rate $\dot{\epsilon}_0 = 1\ s^{-1}$ and the following parameters were used:

$$F_m = 10 \quad W_x = 1{,}6 \quad S = 0{,}8 \quad W_y = 5{,}5 \tag{11.8}$$

11.2   Flow rule

The Kong and Fang model uses the same flow rule as the K&C model

$$g = \sqrt{3J_2} - \omega F(\sigma_{ij}, D) \qquad (11.9)$$

where ω is a parameter between 0 and 1. This rule is partially associative.

The effective plastic strain increment is

$$\Delta \bar{\varepsilon}_p = \sqrt{\frac{2}{3} \Delta \varepsilon_{ij}^p \Delta \varepsilon_{ij}^p} = \sqrt{1 + \frac{2}{9} \left(\omega \frac{dF(\sigma_{ij}, D)}{dP} \right)^2} \Delta \lambda \qquad (11.10)$$

11.3   Modification of Kong-Fang model

Zhang et al (2020) [41] made some improvements and modifications to the original Kong and Fang model.

11.3.1   Modification of residual strength

Numerical simulations with the original Kong and Fang model show that the tunneling diameter is larger than the projectile diameter. This is probably due to an inaccurate description of the residual strength when the concrete is totally damaged. The residual strength is in Zhang et al (2020) modified to

$$\sigma_r = \begin{cases} 0 & P \leq 0 \\ 0{,}7 \, f_c \, (3P/f_c)^{a_3} & 0 < P \leq f_c/3 \\ \dfrac{P}{a_1 + a_2 P} & P > f_c/3 \end{cases} \qquad (11.11)$$

where a_3 is another material parameter.

11.3.2   Introduction of yield strength surface

The original Kong Fang cannot consider compressive strain hardening. This leads to inaccurate prediction of compressive behavior under high confinement. A yield strength surface is therefore introduced.

$$\sigma_y = \begin{cases} \left(3 - \dfrac{9T}{f_{yc}}\right)P + 3T & 0 \le P \le f_{yc}/3 \\[3mm] f_{yc} + \dfrac{P - f_{yc}/3}{a_{1y} + a_{2y}P} & P > f_{yc}/3 \end{cases} \tag{11.12}$$

Modification of current failure surface:

$$Y(\sigma_{ij}, D) = \begin{cases} r'[D(\sigma_r - \sigma_m) + \sigma_m] & P \le 0, \text{tensile} \\ r'[\eta(\sigma_m - \sigma_y) + \sigma_y] & \lambda \le \lambda_m, P > 0, \text{strain} - \text{hardening} \\ r'[\eta(\sigma_m - \sigma_r) + \sigma_r] & \lambda > \lambda_m, P > 0, \text{strain} - \text{softening} \end{cases} \tag{11.13}$$

where η is a scale factor related to the modified equivalent plastic strain λ, and λ_m is the value of λ corresponding to the peak stress.

12   Summary

In this report, a wide range of material models for concrete are discussed. Some of these models were designed for use in finite element codes around 1990. They were later refined to give a better description of concrete, especially for high pressure. In Table 11.1, the major properties of the different material models described in this report are listed.

Yield functions with different number of parameters are discussed. Models with at least three parameters are able to describe shear dilatancy, which is an important property for concrete. After yield is reached, some models for describing plastic flow are described. Some of the models include a "cap-function", which describe the concrete material at high hydrostatic pressures.

As discussed in Chapter 11, it is not straightforward to define a material model which is valid for both impact loads and blast loads. The new model from Kong and Fang tries to combine the best "parts" of existing models.

Table 12.1   Summary of different material models described in this report.

# par. in yield mod.	Model	Yield	EOS	Flow	$\dot{\varepsilon}$	J₃	CAP	Damage	Hardening /Softening	Tensile behavior	Ref
	RHT		P-α		Y	N	Y		Linear crack s.		[21]
	HJC		Piece. lin		Y	N	N			Elastic perfect plastic	[33]
			Piece. lin			Y					[35]
	Impetus			A/N-A		Y					[39]
	Kong and Fang			A/N-A		Y			Comp. strain h.		[40]
				A/N-A		Y		Vol. tensile damage	Exp. Crack s.		[41]
	LS_DYNA				Y	Y	Y	Softening with erosion			[25]
	K & C	**Hyperbolic**		A/N-A		Y	N			No tensile fail	
	Winfrith	**Ottosen**			Y	Y	Y	Smeared crack			
2		**MC**	Lin		N	N	N	N			FFI
			N-A		N	N	N	Softening			[42]
			N-A		N	Y	N	N			[23]
		Drucker-Prager			N						Feenstra et al (1984)
3		**Bresler-Pister**									[8]
		William-Warnke			Y						
		Lubliner		N-A				Anisotropic			[11]
											[12]
		Mentrey William		N-A	Y	Y		N	Based on strain rate		[22]
											[16]
4		**Ottosen**		N-A			Y				[14]
		Hsieh Ting Chen		N-A					Isotropic		Imran et al (2001)
											[20]
		Mises Schleicher									[18]
5		**5 par W-W**									

References

1.   Sjøl and Teland, *Prediction of concrete penetration using Forrestal's formula.* FFI/RAPPORT-99/04415, 1999.

2.   Teland and Sjøl, *An examination and reinterpretation of experimental data behind various empirical equations for penetration into concrete.* Proceedings of the 9th ISIEMS, Berlin, 1999.

3.   Chen, *Plasticity in reinforced concrete.* McGraw-Hill Book Company, 1982.
4.   Babu, Benipal, and Singh, *Constitutive modelling of concrete: An overview.* Asian Journal of civil Engineering, 2005. **6**(4): p. 211-246.

5.   Teland and Svinsås, *Everything you wanted to know about material testing, but were afraid to ask.* FFI/RAPPORT/2003/00155, 2003.

6.   Forrestal and Tzou, *A spherical cavity-expansion penetration model for concrete targets.* Int J Solids Structures, 1997. **34**(31-32): p. 4127-4146.

7.   Abbo and Sloan, *A smooth hyperbolic approximation to the Mohr-coulomb yield criterion.* Computers and structures, 1995. **54**(3): p. 427-441.

8.   Dede and Ayvaz, *Plasticity models for concrete material based on different criteria including Bresler-Pister.* Materials and Design, 2010. **31**: p. 278-286.

9.   William and Warnke, *Constitutive model for the triaxial behaviour of concrete.* Colloquium on Conrete structures subjected to triaxial strresses, IABSE Report, Vol 19, JABSE,Hönggebergs, 1975. **19**: p. 1-30.

10.   Cicekli, *A plasticity-damage model for plain concrete.* LSU Doctorial dissertations 2117, 2006.

11.   Cicekli, Voyiadjis, and Al-Rub, *A plasticity and anisotropic damage model for plain concrete.* Int J of Plasticity, 2007. **23**: p. 1874-1900.

12.   Zhang and Li, *Investigation into Lubliner yield criterion of concrete for 3D simulation.* Engineering Structures, 2012. **44**: p. 122-127.

13.   Ottosen, *A failure criterion for concrete.* Journal of engineering mechanics, 1977.

14.   Zhang, et al., *A constitutive model of concrete based on Ottosen yield criterionb.* Int J of Solids and structures, 2020. **193-194**: p. 79-89.

15.   Hoek and Brown, *Empirical strength criterion for rock masses.* Journal of the geotechnical engineering division, 1980. **September** p. 1013-1035.

16.   Radoslav, *Identification of the parameters of Menetrey-William failure surface of calcium silicate units.* Matrerials Science and Enginbeering, 2017. **245**.

17. Shen, et al., *A new macroscopic criterion of pourous materials with a Mises-Schleicher compressible matrix.* European Journal of Mechanics A/Solids, 2015. **49**: p. 531-538.

18. Durban, Cohen, and Hollander, *Plastic response of porous solids with pressure sensitive matrix.* Mechanics Research Communications, 2010. **37**: p. 636-641.

19. Monchiet and Kondo, *Exact solution of a plastic hollow sphere with a Mises-Schleicher matrix.* International J of Engineering Science, 2012. **51**: p. 168-178.

20. Dede and Ayvaz, *Comparative study of plasticity models for concrete material by using different criteria including Hsieh-Ting-Chen criterion.* Materials and Design, 2010. **31**: p. 1482-1489.

21. Riedel, Thoma, and Hiermaier, *Penetration of Reinforced Concrete by BETA-B-500 Numerical Analysis using a New Macroscopic Concrete Model for Hydrocodes.* Proceedings of the 9th IEMS, Berlin 1999.

22. Grassl, Lundgren, and Gylltoft, *Concrete in compression: A plasticity theory with a novel hardening law.* Int J of Solids and structures, 2002. **39**: p. 5205-5223.

23. Vermeer and d. Borst, *Non-associated plasticity for soils, concrete and rock.* Heron, 1984. **29**(3).

24. Frantziskonis, Desai, and Somasundaram, *Constitutive model for nonassociative behaviour.* Journal of engineering mechanics, 1986. **112**: p. 932-946.

25. *LS DYNA user's manual.* 2007.

26. Saini, Oppong, and Shafei, *Inverstigation of concrete constitutive models for ultra-high performance fiber reinforced concrete under low-velocity impact.* Int J of Impact Engineering, 2021. **157**: p. 103969.

27. Hansson and Skoglund, *Simulation of concrete penetration i 2D and 3D with the RHT material model.* FOI-R-0720-SE, 2002.

28. Heckötter and Sievers, *Comparison of the RHT Concrete material model in LS-DYNA and AUTODYN.* 11th European LS-DYNA Conference 2017, Salzburg, Austria, 2017.

29. Malvar, et al., *A plasticity concrete material model for DYNA3D.* Int J of Impact Engineering, 1997. **19**(9-10): p. 847-873.

30. Magallanes, et al., *Recent improvements to release III of the K&C concrete model.* 11th European LS-DYNA Conference 2017, Salzburg, Austria, 2017.

31. Kong, et al., *Modified K & C model for cratering and scabbing of concrete slab under projectile impact.* Int J of Impact Engineering, 2017. **108**: p. 217-228.

32. Johnson and Cook, *A constitutive model and data for metals subjected to large strains, high strain rates and high temperatures.* Proceedings of the 7th International symposium on ballistics, The Hague, 19-21 April 1983, 1983: p. 541-547.

33. Holmquist, T.J., G.R. Johnson, and W.H. Cook, *A computational constitutive model for concrete subjected to large strains, high strain rates and high pressures.* 14th international symposium on Ballistics, 1993: p. 591-600.

34. Hanchak, S.J., et al., *Perforation of concrete slabs with 48 MPa (7 ksi) and 140 MPa (20 ksi) unconfined compresssive strengths.* Int. Journal of Impact Engineering, 1992. **12**(1): p. 1-7.

35. Polanco-Loria, et al., *Numerical predictions of ballistic limits for concrete slabs using a modified version of the HJC concrete model.* Int J of Impact Engineering, 2008. **35**: p. 290-303.

36. Islam and Liu, *Penetration of concrete targets using a modified Holmquist-Johnson-Cook material model.* Int J of Computational methods, 2013.

37. Kong, Fang, and Peng, *Numerical predictions of cratering and scabbing in concrete slabsa subjected to projectile impact using a modified version of HJC material model.* Int J of Impact Engineering, 2016. **95**: p. 61-71.

38. Weerhejm and v. Doormaal, *Tensile failure of concrete at high loading rates: New test data on strength and fracture energy from intrumented spalling tests.* Int J of Impact Engineering, 2007. **34**: p. 609-626.

39. *Impetus User's Manual.*

40. Kong, et al., *A new material model for concrete subjected to intense dynamic loadings.* Int J og Impact Engineering, 2018. **120**: p. 60-78.

41. Zhang, et al., *Numerical prediction of dynamic failure in concrete targets subjected to projectile impact by a modified kong-Fang material model.* Int J of Impact Engineering, 2020. **144**: p. 103633.

42. Onate, et al., *A constitutive model for cracking of concrete based on the incremental theory of plasticity.* Engineering Computations, 1988. **5**(4): p. 309-319.

About FFI
The Norwegian Defence Research Establishment (FFI) was founded 11th of April 1946. It is organised as an administrative agency subordinate to the Ministry of Defence.
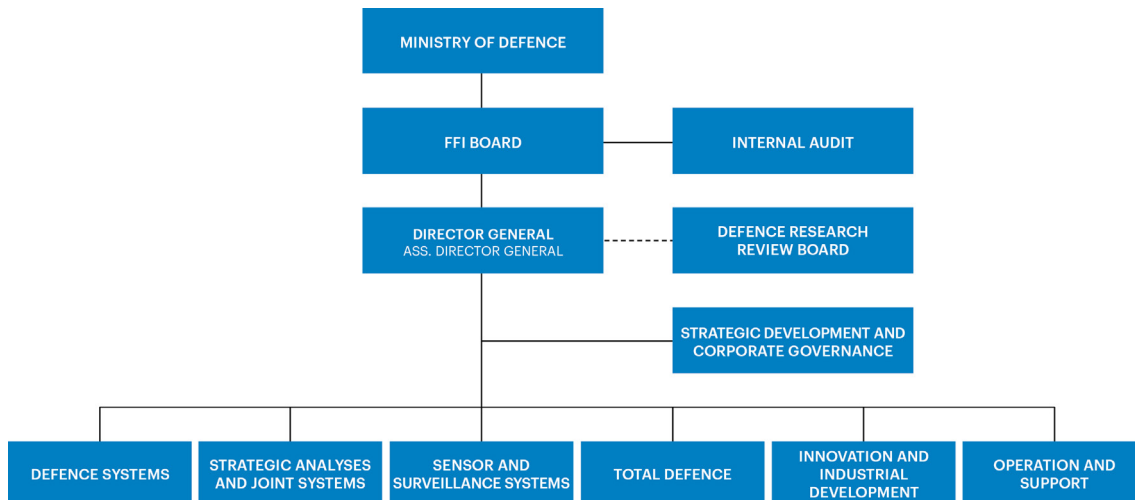
FFI's mission
FFI is the prime institution responsible for defence related research in Norway. Its principal mission is to carry out research and development to meet the requirements of the Armed Forces. FFI has the role of chief adviser to the political and military leadership. In particular, the institute shall focus on aspects of the development in science and technology that can influence our security policy or defence planning.

FFI's vision
FFI turns knowledge and ideas into an efficient defence.

FFI's characteristics
Creative, daring, broad-minded and responsible.

```
                    ┌──────────────────────┐
                    │  MINISTRY OF DEFENCE  │
                    └──────────────────────┘

        ┌──────────────────┐        ┌──────────────────┐
        │     FFI BOARD     │────────│  INTERNAL AUDIT   │
        └──────────────────┘        └──────────────────┘

        ┌──────────────────┐        ┌──────────────────┐
        │ DIRECTOR GENERAL  │ - - - -│  DEFENCE RESEARCH │
        │ASS. DIRECTOR GEN. │        │   REVIEW BOARD    │
        └──────────────────┘        └──────────────────┘

                               ┌───────────────────────────┐
                               │ STRATEGIC DEVELOPMENT AND  │
                               │  CORPORATE GOVERNANCE      │
                               └───────────────────────────┘
```

| DEFENCE SYSTEMS | STRATEGIC ANALYSES AND JOINT SYSTEMS | SENSOR AND SURVEILLANCE SYSTEMS | TOTAL DEFENCE | INNOVATION AND INDUSTRIAL DEVELOPMENT | OPERATION AND SUPPORT |